Heliyon 10 (2024) e26933

Contents lists available at ScienceDirect

Heliyon

journal homepage: www.cell.com/heliyon

Research article

An ultra-compact mechanical antenna based on PTFE highly charged electret for extremely low frequency communications☆

Wenhou Zhang [a], Zongxin Wang [a,*], Zhenxin Cao [a], Xiaoyu Wang [b], Mengjiang Sun [a], Dongning Cui [b], Ying Chen [c], Song Ma [c]

[a] The school of information science and engineering, Southeast University, Nanjing 210000, China
[b] the school of mechanical engineering, Dalian Jiaotong University, Dalian 116000, China
[c] the Southwest China Institute of Electronic Technology,Chengdu 610036, China

ARTICLE INFO

Keywords:
Extremely-low frequencies
Porous thin film electret
Charge
Mechanical antenna

ABSTRACT

—Extremely-Low Frequencies (ELF, 30~300Hz) transmitting antennas in wireless communications are often limited by antenna size and complex impedance matching networks. In this paper, we propose an ultra-small Artificial Electret Type Mechanical Antenna (AETMA), which is composed of a single charge electret and a driving structure, with high radiation efficiency and small size. In order to improve the electric dipole moment of the mechanical antenna, we employ a pin-plate corona polarization technique and a unidirectional stretching treatment to obtain a porous thin-film electret that can stably store a large amount of charge. Its surface charge density can reach 5.355 mC/m^2 and we analyze its surface potential stability. To assess the radiation capability of AETMA, the radiation field models of three kinds of mechanical antennas are established and verified by simulation. Additionally, we simulate and compare the planar electret and curved electret configurations to determine the optimal form of AETMA. The radiation intensity of the planar electret is found to be superior under the same moment of inertia. Finally, a 1m-scale artificial electret antenna is designed based on the optimal model. Comparative analysis with existing rotary mechanical antenna schemes confirms the great potential of the proposed AETMA for portable, miniaturized and high-performance wireless communication devices.

1. Introduction

Extremely Low Frequencies (ELF, 30~300Hz) radio waves are widely used in submarine communication, long-distance communication and cross-domain communication due to their low attenuation and deep penetration characteristics. According to electromagnetic (EM) wave theory, the size of an electric small antenna depends on the wavelength [1]. The conventional ELF antennas are characterized by large size, low flexibility, poor concealment and high cost [2–4], which makes their impractical for applications. Therefore, new methods for generating ELF electromagnetic waves and realizing small-size ELF communication systems have become a hot area of research.

Different from conventional antennas which rely on electrical currents, mechanical antennas (MAs) radiate EM waves by

☆ This work was supported by Equipment Advanced Research Field Foundation (61405180302)

* Corresponding author.
E-mail addresses: 230218649@seu.edu.cn (W. Zhang), wangzx@seu.edu.cn (Z. Wang), caozx@seu.edu.cn (Z. Cao), 99925010@qq.com (X. Wang), 213170963@seu.edu.cn (M. Sun), 531274618@qq.com (D. Cui), chnchenying@163.com (Y. Chen), ma_song@139.com (S. Ma).

https://doi.org/10.1016/j.heliyon.2024.e26933
Received 7 November 2023; Received in revised form 18 February 2024; Accepted 21 February 2024
Available online 6 March 2024

mechanically rotating or oscillating electric and magnetic charges. The research team has proposed several novel methods to generate ELF radiation using the mechanical motion of electric or magnetic charges. This radiation method, which converts mechanical energy into electromagnetic energy without the need for an impedance matching network, has great potential for addressing the challenges associated with large size, complex structure, and highly power consumption. Moreover, it offers the opportunity to enhance the mobility of low-frequency communications.

For the mechanical motion of magnetic dipoles, there are two main types of mechanical antennas (MAs): magnetoelectric and rotating permanent magnet MAs. The magneto-mechanical antenna utilizes the magnetostrictive effect of piezoelectric and magnetostrictive materials. By applying voltage to the PZT-5H piezoelectric material and generating stress to excite the FeGa material, it generates low-frequency EM radiation [5,6]. The rotating permanent magnet type MA produces an alternating magnetic field by rotating the permanent magnet, which generates an oscillating static magnetic field to form EM waves. ELF spinning permanent magnet transmitters were demonstrated in Refs. [7–10]. Efficient modulation techniques for spinning permanent magnet were also explored in Ref. [11], which achieved an 8bit/s frequency shift keying (FSK) modulated signal by changing the frequency of the excitation signal provided to the antenna excitation coil. However, the decay law of the alternating magnetic field generated by the magnetic-charge mechanical antenna in the near field is $1/R^3$, whereas the decay law of the alternating magnetic field generated by the electric-charge mechanical antenna in the near field is $1/R^2$. Therefore the electric-charge mechanical antenna is more suitable for long-distance communications.

Regarding the mechanical movement of electric dipoles, two primary types of MAs are piezoelectric and rotating electret MAs. Piezoelectric MAs employ the piezoelectric effect in materials such as lithium niobate or lead zirconate titanate. By applying a voltage to these materials, an alternating electric field is generated, leading to the electromagnetic radiation [12–14]. The rotating electret type MA generates a time-varying electric field by rotating the electret, which results in an oscillating static electric field and the production of electromagnetic waves [15]. However, when compared to permanent magnet mechanical antennas that can reach a range of 100 m, electret mechanical antennas can only communicate at a range of 10 m. This limitation stems from the relatively weak charge storage capability of natural electret materials (the best electret materials have a charge density of 0.46 mC/m^2 [16]) and piezoelectric to store charge.

To obtain higher charge electret, we unidirectionally stretch polytetrafluoroethylene (PTFE) materials to form more complex defects (such as CO, CH, COH, and CF) to produce more deep traps. This improves the ability of PTFE materials to trap space charge, and this new porous structure can be stabilized to store large amounts of charge [17]. Based on the treated material, we demonstrate a mechanical antenna based on a porous thin-film electret. The antenna utilizes a drive motor to excite positive and negative charge electrets containing a single positive/negative charge electret, which improves the radiation efficiency and reduces the antenna size. Through various theories and multi-physics simulation results, we reveal the relationship between the parameters of porous film PTFE electret and electromagnetic radiation, which establishes a new way and provides a theoretical basis for the development of mechanical antennas. Finally, in this work, we demonstrate an AETMA with 1 m size and compare it with the radiation capability as well as power consumption of other forms of mechanical antennas highlighting the high potential of the proposed AETMA for applications in portable, miniaturized, high-performance wireless communication devices.

In this paper, we optimize the polarization mode and structure of PTFE material so that it can stably store a large amount of charge, and improve the theoretical foundation for future prototype fabrication of electret-type mechanical antennas. Section II describes the optimization method for high charge electret type mechanical antennas and compares the optimized electret material with the raw material. Section III analyzes the equivalent model of an electret mechanical antenna and analyzes the radiated field of the equivalent model. In Section IV, we validate the previous theoretical analysis part of the simulation based on a 1 m size electret. Finally, we present the conclusions and outlook of this paper in Section V, with a comparative analysis of existing mechanical antennas.

2. Analysis and design of artificial electret

The electric dipole type mechanical antenna achieves electrostatic field oscillation by mechanical motion equivalent to that of an electric dipole electret, thus forming electromagnetic waves. However, in our study, we found that not all electrets can be directly equated to electric dipoles. Therefore, we first investigate the classical electret charge distribution and then analyze the artificial electret design based on it.

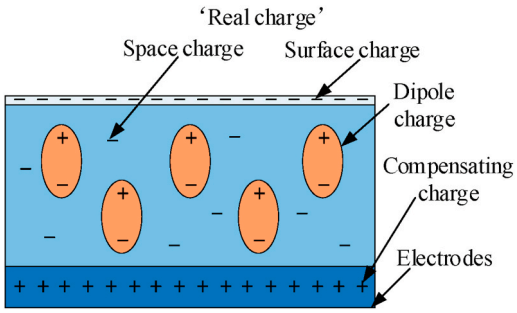

Fig. 1. Schematic diagram of electret charge types and distribution with electrodes.

2.1. Electret working mechanism

The source of the charge stored in the electret is shown in Fig. 1 and can be either the "real charge (space charge)" injected from outside or the polarized charge generated by the directional arrangement of the dipole moment in the electret, or both [18]. The real charges are mainly divided into surface charges captured on or near the surface of the electret and space charges stored inside the electret.

Depending on the electrode and the material properties, the electret charge distribution is mainly shown in Fig. 2. Fig. 2(a) shows a negative polarity electret without electrodes, which shows a relatively strong external and internal electric field because its internal dipole charge is much less than the space charge and has no electrodes; Fig. 2(b) shows an electret with a negative space charge on the surface and a potential barrier with the electrode on one side, generating an internal and external electric field in the body as in the model of Fig. 2(a); Fig. 2(c) shows a polymerized charge electret with surface and interface charges (Maxwell-Wagner charges), which also forms a barrier with the electrode on one side and displays an internal and external electric field; Fig. 2(d) shows a double-sided electrode electret with coexistence of dipole charge and space charge, which only exhibits a relatively strong internal electric field due to the characteristic of carrying electrodes on both sides. Considering that the mechanical antenna needs electret that can generate strong external electric field, the aforementioned electrets are suitable for use in electret type mechanical antenna except for double-electrode dipole charge electrets.

2.2. Artificial electret design

The ability of electrets to store charge is attributed to the presence of traps within the material. These traps are primarily associated with defects in the lattice structure, intergranular gaps, intermolecular chain spacing, and porosity. We prepare the electret using the corona polarization technique, and the external charge generated is mainly the body charge captured by the trap. If the trapped charge energy is smaller than the trap's own binding energy level, these body charges will not be able to break free from the trap, thus forming an electret that remains polarized for a long time. In order to fully polarize the electret and thus increase the overall number of charges stored in the electret, we used the pin-plate corona polarization technique as shown in Fig. 3.

As shown in Fig. 3, the needle plate corona polarization mainly ionizes the air around the tip electrode by high voltage, generating a large number of charged ions, which are uniformly captured by the electret under the action of electric field through the grid. The polarization of the electret material is achieved by controlling the polarity of the high-voltage power supply. Positive or negative corona polarization can be utilized to polarize the electret material accordingly. The tip voltage is positive for positive corona polarization (Fig. 3(a)), and the charge of the electret is positive; the tip voltage is negative for negative corona polarization (Fig. 3(b)), and the charge of the electret is negative. In corona polarization, the corona voltage is typically set at 10 kV, and the charging time is set to 10 min. Additionally, the grid voltage is set at 1 kV.

To improve the stability of stored charges in electret materials, the PTFE film is stretched unidirectionally at a certain temperature to form more complex defects, resulting in a deep trap containing a higher concentration of space charge. The thickness of the porous PTFE film is 30 μm, the pore size is 5–10 μm, and the porosity is 70%. The advantages of the storage charge stability of porous PTFE films are determined by studying the decay of the surface potential with time for porous and non-porous PTFE films as well as for non-porous FEP films, the results of which are shown in Fig. 4.

As can be seen from Fig. 4, the equivalent potential of porous PTFE films aged at 200 °C for 5h after constant pressure negative corona polarization at room temperature was basically unchanged and maintained at more than 99% of the initial value. However, the equivalent potentials of non-porous PTFE and FEP films were reduced to 78% and 25% of the initial values under the same conditions.

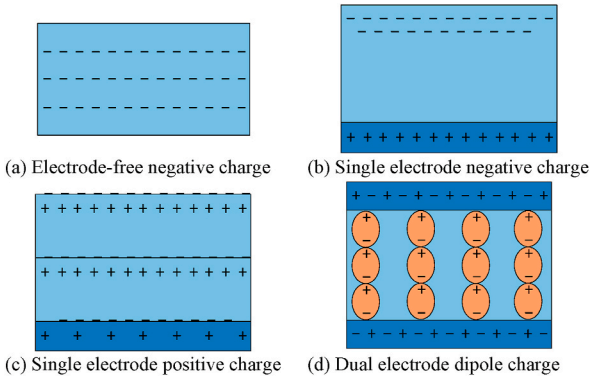

Fig. 2. Schematic diagram of charge distribution in classical electret
(a) Electrode-free negative charge
(b) Single electrode negative charge
(c) Single electrode positive charge
(d) Dual electrode dipole charge.

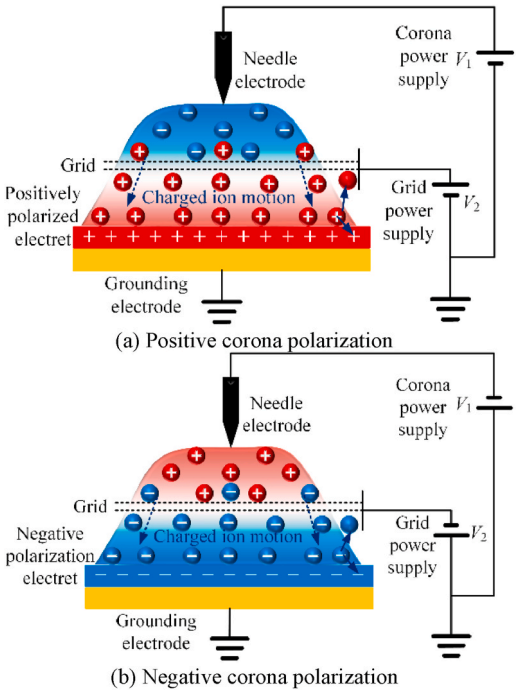

Fig. 3. Schematic diagram of electret needle-plate corona polarization
(a) Positive corona polarization
(b) Negative corona polarization.

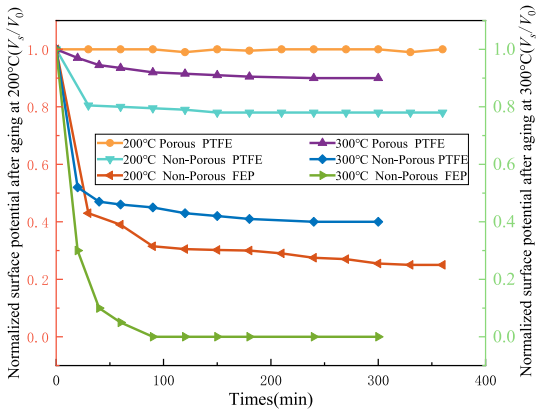

Fig. 4. Isothermal surface potential decay curve after normal temperature and constant pressure negative corona polarization.

After aging at 300 °C for 5h, the equivalent potential of porous PTFE films decreased to 90% of the initial value. The equivalent potentials of non-porous PTFE and FEP films were reduced to 40% and 0% of the initial values. Therefore, unidirectionally stretched porous PTFE films have the best electret charge storage stability. Interestingly, the gate voltage required for positive corona polarization of the porous PTFE film is 110% of that required for negative corona polarization, and the equivalent potential base of the porous PTFE film aging at 200 °C for 5h remains above 90% of the initial value [17]. Therefore, the negative corona-polarized PTFE is more suitable as an electret mechanical antenna transmitting source.

3. AETMA radiation mechanism

3.1. AETMA equivalent model

Based on the previous analysis of electrets and their role in mechanical antennas, the design of artificial electrets can take three different forms, as illustrated in Fig. 5. Attaching the electret to an insulating plate and rotating the electret with a motor is a viable

AETMA solution. Fig. 5(a) shows a negative monopole type electret mechanical antenna with negative corona polarization electret; Fig. 5(b) shows a positive monopole type electret mechanical antenna with positive corona polarization electret; Fig. 5(c) shows an electric dipole type electret mechanical antenna with negative corona polarization and positive corona polarization electret.

The electret mechanical antenna shown in Fig. 5(a) and (b) can be equated to an electric monopole rotation as shown in Fig. 6(a). The electric dipole type antenna shown in Fig. 5(c) can be equated to a rotating electric dipole, as shown in Fig. 6(b). The charge of the equivalent model can be expressed as:

$$q = \frac{\varepsilon\varepsilon_0}{L}\alpha V_s S. \tag{1}$$

where, ε is the dielectric constant of the electret material; ε_0 is the vacuum dielectric constant; L is the thickness of the electret material; α charge storage efficiency; V_s is the isothermal surface potential of the electret; S is the area of the electret.

3.2. AETMA time-varying field model and characteristic analysis

3.2.1. AETMA time-varying field model in free space

As shown in Fig. 6(a), a charge of charge q rotates in the yoz plane with a radius of rotation a, an angular frequency ω, and $a\omega \ll c$. The rotating electric dipole can be equivalent to two orthogonal vibrating electric dipoles, and the charge, frequency and amplitude of the vibrating electric dipole are the same as the corresponding parameters of the rotating electric dipole. Thus, the electrode moment of a rotating electric dipole can be expressed as:

$$\boldsymbol{p}_{sc} = qa(\cos(\omega t)\boldsymbol{z} - \sin(\omega t)\boldsymbol{y}). \tag{2}$$

where, $\boldsymbol{y}$ and $\boldsymbol{x}$ are the unit vectors in the y-direction and x-direction, respectively.

As shown in Fig. 6(c), an electric dipole of charge q rotates in the yoz plane with a radius of rotation a, an angular frequency ω, and $a\omega \ll c$. The rotating electric dipole can be equated to two orthogonal vibrating electric dipoles with the same charge, vibration frequency and vibration amplitude as the corresponding parameters of the rotating electric dipole. Therefore, the electrode moment of a rotating electric dipole can be expressed as:

$$\boldsymbol{p}_{ed} = 2qa(\cos(\omega t)\boldsymbol{z} - \sin(\omega t)\boldsymbol{y}). \tag{3}$$

Based on the time-varying field generated by the vibrating electric dipole moment [1] and the mapping relationship between

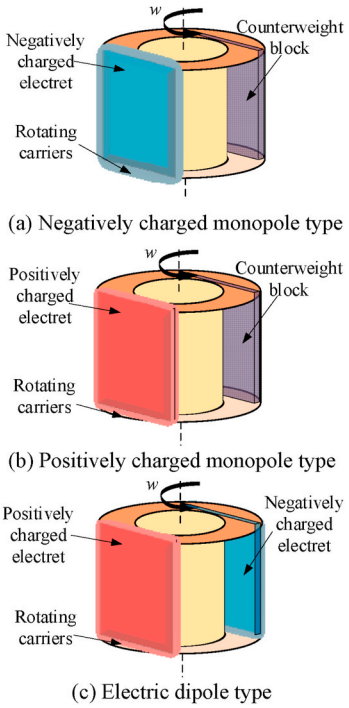

Fig. 5. Artificial electret type mechanical antenna
(a) Negatively charged monopole type
(b) Positively charged monopole type
(c) Electric dipole type.

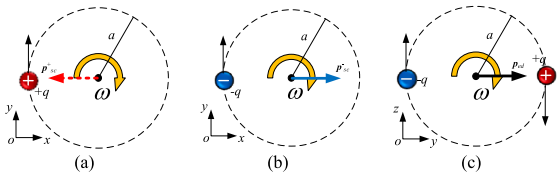

Fig. 6. Equivalent model of artificial electret mechanical antenna (a) Rotating positive electropositive monopole; (b) Rotating positive electropositive monopole; (c) Rotating electric dipole.

rotational motion and simple harmonic vibration (equation (2)(3)), the time-varying field generated by AETMA can be expressed as:

$$\begin{cases} \boldsymbol{B}_{sc} = -\dfrac{\mu_0 k^2 \omega q a e^{-\mathrm{j}kR}}{4\pi} \begin{bmatrix} \dfrac{1}{kR} - \\ \dfrac{\mathrm{j}}{(kR)^2} \end{bmatrix} \times \begin{bmatrix} \begin{pmatrix} \sin\theta - \\ \mathrm{j}\cos\theta\sin\varphi \end{pmatrix} \boldsymbol{a}_\varphi \\ +j\cos\varphi \boldsymbol{a}_\theta \end{bmatrix} \\ \boldsymbol{E}_{sc} = \dfrac{\eta_0 k^2 \omega q a e^{-\mathrm{j}kR}}{4\pi} \begin{Bmatrix} 2\begin{bmatrix} \dfrac{\mathrm{j}}{(kR)^2} + \\ \dfrac{1}{(kR)^3} \end{bmatrix} \begin{pmatrix} \cos\theta + \\ \mathrm{j}\sin\theta\sin\varphi \end{pmatrix} \boldsymbol{a}_R \\ -\mathrm{j}\cos\varphi \boldsymbol{a}_\varphi - \begin{bmatrix} \dfrac{1}{kR} - \dfrac{\mathrm{j}}{(kR)^2} \\ -\dfrac{1}{(kR)^3} \end{bmatrix} \\ (\sin\theta - \mathrm{j}\cos\theta\sin\varphi)\boldsymbol{a}_\theta \end{Bmatrix} \end{cases} . \tag{4}$$

$$\begin{cases} \boldsymbol{B}_{ed} = -\dfrac{\mu_0 k^2 \omega q a e^{-\mathrm{j}kR}}{2\pi} \begin{bmatrix} \dfrac{1}{kR} - \\ \dfrac{\mathrm{j}}{(kR)^2} \end{bmatrix} \times \begin{bmatrix} \begin{pmatrix} \sin\theta - \\ \mathrm{j}\cos\theta\sin\varphi \end{pmatrix} \boldsymbol{a}_\varphi \\ +j\cos\varphi \boldsymbol{a}_\theta \end{bmatrix} \\ \boldsymbol{E}_{ed} = \dfrac{\eta_0 k^2 \omega q a e^{-\mathrm{j}kR}}{2\pi} \begin{Bmatrix} 2\begin{bmatrix} \dfrac{\mathrm{j}}{(kR)^2} + \\ \dfrac{1}{(kR)^3} \end{bmatrix} \begin{pmatrix} \cos\theta + \\ \mathrm{j}\sin\theta\sin\varphi \end{pmatrix} \boldsymbol{a}_R \\ -\mathrm{j}\cos\varphi \boldsymbol{a}_\varphi - \begin{bmatrix} \dfrac{1}{kR} - \dfrac{\mathrm{j}}{(kR)^2} \\ -\dfrac{1}{(kR)^3} \end{bmatrix} \\ (\sin\theta - \mathrm{j}\cos\theta\sin\varphi)\boldsymbol{a}_\theta \end{Bmatrix} \end{cases} . \tag{5}$$

where, k is the propagation constant; R is the distance between the field point and the source point; θ is the polar angle of the field point; φ is the azimuthal angle of the field point; $\boldsymbol{a_R}$, $\boldsymbol{a_\theta}$, $\boldsymbol{a_\varphi}$ are the unit vectors of the right subscript variable; μ_0 is the vacuum permeability; $\eta_0 = c\mu_0$ is the free-space wave impedance.

According to equations (4) and (5), in AETMA antenna, the time-varying field amplitude of the electric dipole type is twice that of the electric monopole type, and other characteristics are consistent.

3.2.2. AETMA field distribution characteristics

In the near-field region, since $kr \ll 1$,$e^{-\mathrm{j}kr} \approx 1$, the lower power of 1/(kr) can be neglected, the near-field time-varying field of AETMA can be expressed as:

$$\begin{cases} \boldsymbol{B}_{sc\_near} = -\dfrac{\mathrm{j}\mu_0\omega qa}{4\pi R^2} \times \begin{bmatrix} (\sin\theta - \mathrm{j}\cos\theta\sin\varphi)\boldsymbol{a}_\varphi \\ +j\cos\varphi\boldsymbol{a}_\theta \end{bmatrix} \\ \boldsymbol{E}_{sc\_near} = \dfrac{\eta_0 cqa}{4\pi R^3} \begin{Bmatrix} 2(\cos\theta + \mathrm{j}\sin\theta\sin\varphi)\boldsymbol{a}_R \\ +(\sin\theta - \mathrm{j}\cos\theta\sin\varphi)\boldsymbol{a}_\theta \\ -\mathrm{j}\cos\varphi\boldsymbol{a}_\varphi \end{Bmatrix} \end{cases} . \tag{6}$$

$$\begin{cases} \boldsymbol{B}_{ed\_near} = -\dfrac{\mathrm{j}\mu_0\omega qa}{2\pi R^2} \times \begin{bmatrix} (\sin\theta - \mathrm{j}\cos\theta\sin\varphi)\boldsymbol{a}_\varphi \\ +j\cos\varphi\boldsymbol{a}_\theta \end{bmatrix} \\ \boldsymbol{E}_{ed\_near} = \dfrac{\eta_0 cqa}{2\pi R^3} \begin{Bmatrix} 2(\cos\theta + \mathrm{j}\sin\theta\sin\varphi)\boldsymbol{a}_R \\ +(\sin\theta - \mathrm{j}\cos\theta\sin\varphi)\boldsymbol{a}_\theta \\ -\mathrm{j}\cos\varphi\boldsymbol{a}_\varphi \end{Bmatrix} \end{cases} . \tag{7}$$

From equations (6) and (7), the near-area time-varying magnetic field of AETMA has both $\boldsymbol{a}_\theta$ and $\boldsymbol{a}_\varphi$ components and has the maximum near-area magnetic field in the *xoy* plane.

In the far-field region, since $kr \gg 1, e^{-\mathrm{j}kr} \approx 1$, the higher power of 1/(kr) can be neglected, the far-field time-varying field of AETMA can be expressed as:

$$\begin{cases} \boldsymbol{B}_{sc\_far} = -\dfrac{\mu_0\omega^2 qae^{-\mathrm{j}kR}}{4\pi cR} \times \begin{bmatrix} (\sin\theta - \mathrm{j}\cos\theta\sin\varphi)\boldsymbol{a}_\varphi \\ +j\cos\varphi\boldsymbol{a}_\theta \end{bmatrix} \\ \boldsymbol{E}_{sc\_far} = \dfrac{\eta_0\omega^2 qae^{-\mathrm{j}kR}}{4\pi cR} \begin{Bmatrix} -\mathrm{j}\cos\varphi\boldsymbol{a}_\varphi - \\ (\sin\theta - \mathrm{j}\cos\theta\sin\varphi)\boldsymbol{a}_\theta \end{Bmatrix} \end{cases} . \tag{8}$$

$$\begin{cases} \boldsymbol{B}_{ed\_far} = -\dfrac{\mu_0\omega^2 qae^{-\mathrm{j}kR}}{2\pi cR} \times \begin{bmatrix} (\sin\theta - \mathrm{j}\cos\theta\sin\varphi)\boldsymbol{a}_\varphi \\ +j\cos\varphi\boldsymbol{a}_\theta \end{bmatrix} \\ \boldsymbol{E}_{ed\_far} = \dfrac{\eta_0\omega^2 qae^{-\mathrm{j}kR}}{2\pi cR} \begin{Bmatrix} -\mathrm{j}\cos\varphi\boldsymbol{a}_\varphi - \\ (\sin\theta - \mathrm{j}\cos\theta\sin\varphi)\boldsymbol{a}_\theta \end{Bmatrix} \end{cases} . \tag{9}$$

According to equations (8) and (9), the far-region time-varying electromagnetic field of AETMA is a spherical wave whose amplitude decays with 1/R and whose phase is the same.

At present, the low-frequency communication mainly uses magnetic receiving technology, so the time-varying magnetic field generated by AETMA in free space is mainly analyzed. From the above analysis, the time-varying magnetic field generated by AETMA shows different attenuation characteristics in the near-field region and far-field region as the communication distance R increases. A square porous PTFE electret with a 1 m size was selected as the radiation source with a dielectric constant of 2.1. From equation (1), the charge of the porous PTFE electret in subsection 1 is 5.355 mC. Assuming that the distance from the center of rotation to the electret in Fig. 5 is 0.5 m, the time-varying magnetic field decay characteristic curve generated by the electric dipole antenna is shown in Fig. 7.

As shown in Fig. 7, the near-field region of AETMA has a faster fading rate ($1/R^2$) as the communication distance increases. Higher frequencies have stronger near-zone magnetic fields, but have faster decay rates in seawater. At a frequency of 300Hz, the near-field

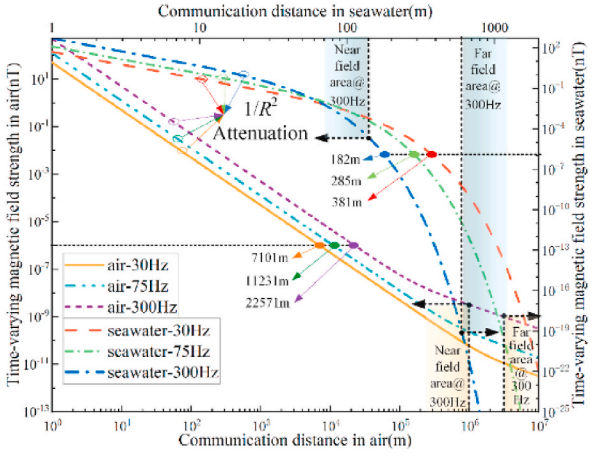

Fig. 7. Time-varying magnetic field attenuation characteristics of electric dipole antenna.

region of AETMA is less than 10^6 m (one electromagnetic wave wavelength) in air and less than 158 m (one electromagnetic wave wavelength) in seawater. When the detection sensitivity of the magnetic sensor is 1 fT, the farthest communication distance of AETMA working in the extremely low frequency band is 22.57 km in the air and 381 m in the sea water.

3.2.3. Effect of frequency on the radiation performance of AETMA

Frequency is one of the crucial factors in low-frequency applications, so this section analyzes the effect of different operating frequencies on the radiation performance of AETMA based on the above design artificial electret, and the results are shown in Fig. 8.

The six curves in Fig. 8 represent six different operating frequencies, which generate time-varying magnetic fields with the same decaying trend with increasing distance. In Fig. 9, it is further shown that the time-varying magnetic fields generated by different operating frequencies are linearly related at the same distance (5 km). Therefore, the AETMA radiation theory in this paper can be applied to ELF. Since the penetration performance of ELF band in lossy media is better than that of other bands in LF [19], this paper focuses on the 75Hz frequency point for the above analysis.

4. AETMA simulation analysis

In this paper, the radiation properties of AETMA are investigated using the multiphysics field simulation software COMSOL Multiphysics. As shown in Fig. 10, a three-dimensional rotation model is adopted in which the artificial electret is placed parallel to both sides of the *xoz* plane. The outer enclosure of the artificial electret is the rotation domain, the air domain, and the infinite element domain. It is worth noting that the middle area of the artificial electret must be set to be completely insulated. The electret material on both sides is always PTFE material, and the electret is positively charged in the negative *y*-axis direction and negatively charged or grounded in the positive *y*-axis direction. The electret motion is controlled in the simulation by controlling the frequency of the rotational domain.

4.1. AETMA time-varying field directionality simulation

From equations (6) and (7), the near-zone time-varying magnetic field of AETMA has the maximum near-zone magnetic field in the *xoy* plane. Low-frequency magnetic sensors mostly use planar coils, so the study of the magnitude of each component of the near-zone time-varying magnetic field is particularly important. Based on the model shown in Fig. 5, the magnetic field distribution generated by monopole type and dipole type AETMA was investigated and the results are shown in Fig. 11.

In the simulation, the operating frequency is 75Hz, the charge is 5.355 mC, and the electret area is 1 m^2. As can be seen from Fig. 11, the generated magnetic field varies periodically with time. When AETMA operates, the total magnetic field radiates uniformly in a horizontal direction, which means that AETMA can be considered as omnidirectional. The maximum values of the *x* and *y* components of the time-varying magnetic field lie on $\pi/4+k\pi/2$ and $k\pi/2$ (k = 0,1,2), respectively, and the *z* component is essentially zero. The time-varying magnetic field of the monopole type is half that of the dipole type, which is consistent with the theoretical analysis.

4.2. Effect of frequency on the time-varying field of AETMA

In order to verify that the electret mechanical antenna is affected by the rotational speed, we simulated the variation of time-varying magnetic field strength in air with different rotational speed. The simulation setup is consistent with Part A except for the electret rotational speed, where the receiving point is 100 m from the center of rotation. The simulation results are shown in Fig. 12. We performed a linear fit to the simulated data, and the fitted curve is a standard positively proportional curve, which well verifies the correctness of the theoretical model.

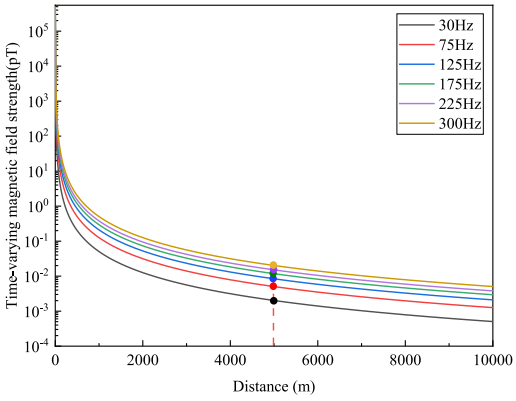

Fig. 8. Influence curve of frequency on AETMA radiation performance.

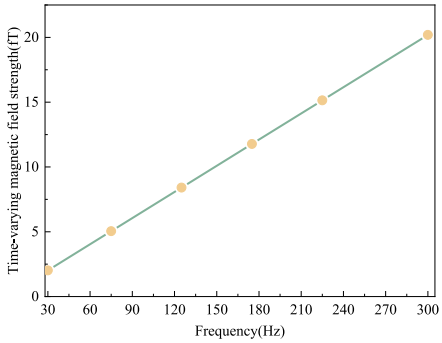

Fig. 9. Relationship between frequency and time-varying magnetic field intensity at the same distance.

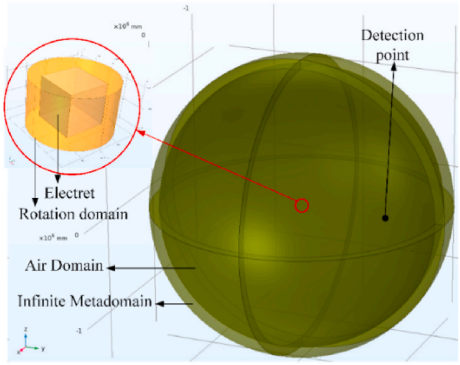

Fig. 10. Simulation model diagram.

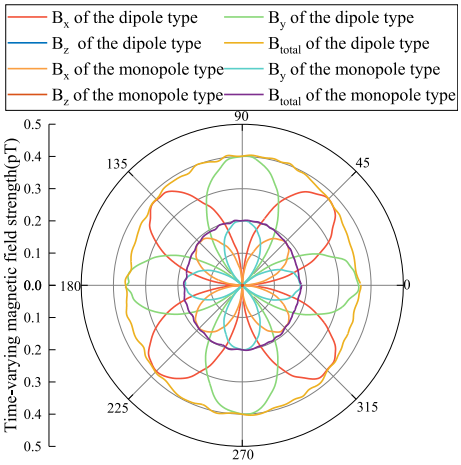

Fig. 11. Magnetic field distribution of AETMA in the xoy plane at different rotation angles.

4.3. AETMA structure optimization

To further explore the optimal structure of AETMA, the same emitter shape as in the previous section, Fig. 13 depicts the type of emitter when the electret film is located on the surface of the rotating fixture. When the electret film is located on the surface of the rotating fixture, the total area of the electret film increases with the same rotational inertia. Fig. 14 depicts the distribution of the magnetic field generated by AETMA shown in Fig. 13.

In the simulation, the operating frequency is 75Hz, the charge is 5.355 mC, and the electret area is 1.58 m^2. As can be seen from Fig. 14, the magnetic field generated by the curved electret type mechanical antenna varies periodically with time, and the distribution law is the same as that of the planar electret type mechanical antenna. Compared with Fig. 11, the time-varying magnetic field

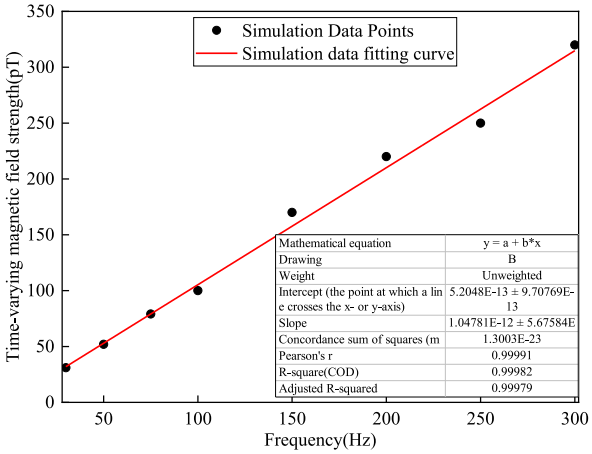

Fig. 12. Rotational speed versus time-varying magnetic field strength.

intensity generated by the curved electret mechanical antenna is half that of the planar electret mechanical antenna. Therefore, the best structural form of AETMA is planar electret.

4.4. AETMA time-varying field attenuation simulation

In order to verify the transmission performance of the electret mechanical antenna, based on the aforementioned planar type electret mechanical antenna with the 1 m size, the attenuation of time-varying magnetic field intensity in the air was simulated, and the results were shown in Fig. 15. As can be seen from Fig. 15, the decay law of the time-varying magnetic field generated by the dipole-type mechanical antenna in the air is basically consistent with the theoretical curve. When the time-varying magnetic field strength is 1 pT, the dipole type electret mechanical antenna can complete the wireless communication at a distance of 700 m. The reason why the simulated data points in Fig. 15 are larger than the theoretical values is that there is a certain deviation between the outer surface of the infinite element domain and the ideal infinity.

5. Conclusion

In this paper, we propose a new rotating electret mechanical antenna that uses corona charging technique to generate a large and stable charge in porous PTFE material. The electromagnetic generation mechanism and the AETMA characteristics are discussed in four aspects: material, charging technology, structure and operation mode. A series of simulations based on multi-physics field simulation software verified the correctness of the concept. The operating frequency is controlled by the rotational frequency, and the time-varying magnetic field strength increases linearly with increasing frequency. Based on the same moment of inertia, two types of electret structures are simulated and the planar type electret is determined to be the optimal model. The simulation results verify the feasibility of the proposed porous PTFE material electret mechanical antenna to radiate electromagnetic waves in the ELF band. Finally, based on the existing rotating mechanical antenna in the 1 m scale range, the radiation intensity is summarized as shown in Table 1.

As can be seen from Table 1, the radiation capacity of the rotating permanent magnet type mechanical antenna is much higher than the radiation capacity of the rotating electret type mechanical antenna under the antenna size of 1 m scale. However, the rotating

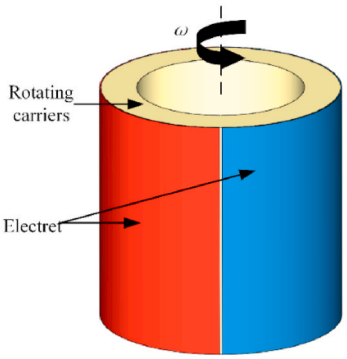

Fig. 13. Electret model on the surface of the rotating fixture.

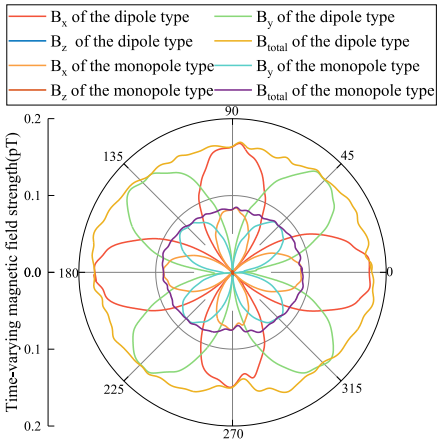

Fig. 14. Magnetic field distribution of electret antenna located on the surface of rotating fixture at different rotation angles in xoy plane.

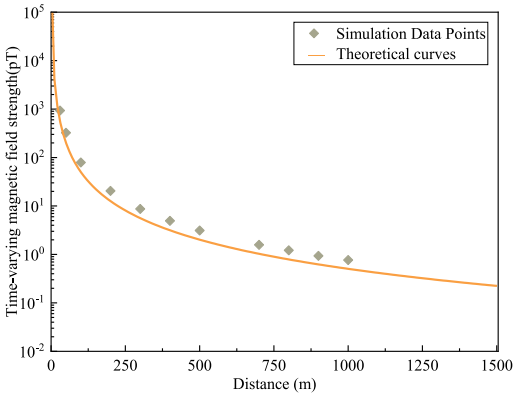

Fig. 15. Simulation results and theoretical curves of attenuation characteristics.

electret type mechanical antenna radiation source is the electret film, which weighs 1/119k of a permanent magnet at a size of 1 m. The power loss of a mechanical antenna is proportional to the weight of the radiating source. Thus the power loss of the permanent magnet mechanical antenna is 119k times that of the electret mechanical antenna. At the cost of such a large power consumption, the increase in communication capability is less than 1000 times, which is clearly inefficient for a transmitting antenna. For the electret type mechanical antenna, this paper is compared with the literature [16], and the radiation capacity of this paper is increased by a factor of 10 for the same size. Besides the time-varying magnetic field of the rotating electret mechanical antenna decreases by the quadratic of the communication distance. Therefore, the electret antenna proposed in this paper will bring great improvement to ELF wireless communication in terms of volume, weight and long-range transmission.

Table 1
Comparison of the performance of rotating mechanical antennas of different research teams.

References	Materials	Size	Operating frequency/Hz	Time-varying magnetic field strength in the literature	1 m scale communication distance @1 pT
[9]	Permanent magnets NdFeB	3 cm^3	500	200 fT@128 m	5.19 km
[10]		3627 cm^3	75	1 pT@200 m	1.3 km
[20]		105 cm^3	1031	28.2pT@30m	1.94 km
[21]		216 cm^3	75	0.3nT@80m	5.41 km
[7]		188.4 cm^3	30	4 nT@10 m	2.77 km
[16]	FEP Electret	196.35 cm^2	30	0.9nT@0.3m	64 m
Article	Porous PTFE Electret	1 m^2	75	700 m@1 pT	700 m

Data Availability

The data used to support the findings of thisstudy are included within the article.

CRediT authorship contribution statement

Wenhou Zhang: Writing – review & editing, Writing – original draft, Validation, Software, Methodology, Investigation, Formal analysis, Data curation, Conceptualization. **Zongxin Wang:** Resources, Project administration, Funding acquisition, Conceptualization. **Zhenxin Cao:** Validation, Funding acquisition, Conceptualization. **Xiaoyu Wang:** Visualization, Validation, Funding acquisition, Conceptualization. **Mengjiang Sun:** Validation. **Dongning Cui:** Visualization, Validation. **Ying Chen:** Funding acquisition. **Song Ma:** Funding acquisition.

Declaration of competing interest

The authors declare that they have no known competing financial interests or personal relationships that could have appeared to influence the work reported in this paper.

Acknowledgments

This work was supported by the Equipment Advance Research Fund (No. 61405180302)

References

[1] C.A. Balanis, Antenna Theory: Analysis and Design, Wiley, Hoboken, NJ, USA, 2005 ch. 5.
[2] N.K. Uzunoglu, S.J. Kouridakis, Radiation of very low and extremely low frequencies (VLF & ELF) by a natural antenna based on an island or a peninsula structure, URSI Radio Science Bulletin 308 (2004) 7–12. March 2004.
[3] M. Morgan, An island as a natural very-low-frequency transmitting antenna, IEEE Transactions on Antennas and Propagation[J] 8 (5) (Sep. 1960) 528–530.
[4] R. Barr, W. Ireland, Low-frequency input impedance of a very large loop antenna with a mountain core, in: IEEE Proceedings H - Microwaves, Antennas and Propagation, vol. 140, Apr. 1993, pp. 84–90, 2.
[5] J.D. Schneider, J.P. Domann, M.K. Panduranga, et al., Experimental demonstration and operating principles of a multiferroic antenna, J. Appl. Phys. 126 (22) (Dec. 2019) 1–6.
[6] J.D. Schneider, J.P. Domann, M.K. Panduranga, et al., Experimental demonstration and operating principles of a multiferroic antenna, J. Appl. Phys. 126 (22) (Dec. 2019) 1–6.
[7] Y. Liu, S. Gong, Q. Liu, et al., A mechanical transmitter for Undersea magnetic Induction communication, IEEE Trans. Antenn. Propag. 69 (10) (Oct. 2021) 6391–6400.
[8] X.Y. Wang, W.H. Zhang, X. Zhou, et al., Radiation characteristics of rotating magnetic dipole Super-low frequency transmitting antenna, Acta Armamentarii 41 (10) (Jul. 2020) 2055–2062.
[9] H.C. Burch, A. Garraud, M.F. Mitchell, et al., Experimental generation of ELF radio signals using a rotating magnet, IEEE Trans. Antenn. Propag. 66 (11) (Nov. 2018) 6265–6272.
[10] J. Han, J.P. Geng, H. Wu, et al., The ultra-compact ELF magneto-mechanical transmission antenna with the speed modulated EM signal based on three-phase Induction motor, IEEE Trans. Antenn. Propag. 69 (9) (Sep. 2021) 5286–5296.
[11] O.C. Fa Wole, M. Tabib-Azar, An Electromechanically modulated permanent magnet antenna for wireless communication in Harsh electromagnetic Environment, IEEE Trans. Antenn. Propag. 65 (12) (Dec. 2017) 6297–6936.
[12] M.A. Kemp, M. Franzi, A. Haase, et al., A high Q piezoelectric resonator as a portable VLF transmitter, Nat. Commun. 10 (1) (Dec. 2019).
[13] A.E. Hassanien, M. Breen, M.H. Li, et al., Acoustically driven electromagnetic radiating elements, Sci. Rep. 10 (1) (2022).
[14] J. Xu, J. Cao, M. Guo, et al., Metamaterial mechanical antenna for very low frequency wireless communication, Advanced Composites and Hybrid Materials 4 (3) (May. 2021) 761–767.
[15] C. Wang, Y. Cui, X. Song, et al., Model, design, and testing of an electret-based portable transmitter for low-frequency applications, IEEE Trans. Antenn. Propag. 69 (9) (Sep. 2021) 5305–5314.
[16] Y. Cui, M. Wu, Z. Li, et al., A miniaturized mechanical antenna based on FEP/THV unipolar electrets for extremely low frequency transmission, Microsystems \Nanoengineering 8 (1) (2022) 1–11.
[17] Z.F. Xia, Y.L. Qiu, Y.W. Zhang, The charge storage stability of porous polytetrafluoroethy lene film electret, Acta Physica Sinica 2 (2002) 389–394.
[18] B. Gross, R. Gerhard-Multhaupt, A. Berraissoul, et al., Electron-beam poling of piezoelectric polymer electrets, Journal of Applied Physics 62 (4) (1987) 1429–1432.
[19] H. E Rowe, Extremely low frequency (ELF) communication to submarines, IEEE Trans. Commun. 22 (4) (1974) 371–385.
[20] F. Fereidoony, S. Nagaraja, J. Santos, et al., Efficient ULF transmission utilizing Stacked magnetic Pendulum Array, IEEE Transactions on Antennas and Propagation 70 (1) (2021) 585–597.
[21] W. Zhang, Z. Cao, X. Wang, et al., Design, Array, and test of Super-low-frequency mechanical antenna based on permanent magnet, IEEE Transactions on Antennas and Propagation 71 (3) (March 2023) 2321–2329.